ELSEVIER

Biophysical Chemistry 78 (1999) 69–88

Biophysical Chemistry

# Effect of artificial periodicity in simulations of biomolecules under Ewald boundary conditions: a continuum electrostatics study

P.H. Hünenberger [a,*], J.A. McCammon [a,b]

[a] *Department of Chemistry and Biochemistry, University of California at San Diego, 9500 Gilman Drive, La Jolla, CA 92093–0365, USA*

[b] *Department of Pharmacology, University of California at San Diego, 9500 Gilman Drive, La Jolla, CA 92093–0365, USA*

Received 17 September 1998; received in revised form 31 December 1998; accepted 31 December 1998

**Abstract**

Ewald and related methods are nowadays routinely used in explicit-solvent simulations of biomolecules, although they impose an artificial periodicity in systems which are inherently non-periodic. The consequences of this approximation should be assessed, since they may crucially affect the reliability of computer simulations under Ewald boundary conditions. In the present study we use a method based on continuum electrostatics to investigate the nature and magnitude of possible periodicity-induced artifacts on the potentials of mean force for conformational equilibria in biomolecules. Three model systems and pathways are considered: polyalanine oligopeptides (unfolding), a DNA tetranucleotide (separation of the strands), and the protein Sac7d (conformations from a molecular dynamics simulation). Artificial periodicity may significantly affect these conformational equilibria, in each case stabilizing the most compact conformation of the biomolecule. Three factors enhance periodicity-induced artifacts: (i) a solvent of low dielectric permittivity; (ii) a solute size which is non-negligible compared to the size of the unit cell; and (iii) a non-neutral solute. Neither the neutrality of the solute nor the absence of charge pairs at distances exceeding half the edge of the unit cell do guarantee the absence of artifacts. 

*Keywords:* Continuum electrostatics; Periodic boundary conditions; Ewald summation; Conformational equilibria

* Corresponding author. Tel.: +1 619 822 1469; fax: +1 619 534 7042; e-mail: phunenbe@ucsd.edu

0301-4622/99/$ - see front matter 
PII: S0301-4622(99)00007-1

## 1. Introduction

The treatment of long-range electrostatic interactions in molecular simulations of liquids and solutions is an area of ongoing research [1–5], for three main reasons: (i) approximations made in the treatment of electrostatic interactions are often among the most severe in a simulation procedure; (ii) many simulated observables are extremely sensitive to this treatment; and (iii) the calculation of electrostatic interactions is usually the most expensive part of a simulation. To avoid the presence of an interface to vacuum, explicit-solvent simulations of (bio-)molecules are commonly performed under periodic boundary conditions. In this case, the electrostatic interactions can be computed in either of two ways: (i) by truncating the pairwise Coulomb interactions at a convenient cutoff distance [6], or (ii) by using lattice summation methods [6–17]. Both choices rely on critical approximations: in the first case the neglect of Coulomb interactions beyond the cutoff distance, and in the second case the exact periodicity of the system. Due to the sensitivity of many simulated observables on the treatment of electrostatic interactions, approximations made in their calculation may crucially affect the reliability of a computer simulation. It is therefore of importance to investigate the nature and magnitude of possible artifacts linked with both of the above choices.

The severe artifacts caused by cutoff truncation in the simulations of liquids [18,19], and solvated ions [20–23], ion pairs [24–30], and biomolecules [31–34] are well documented. The use of switching or shifting functions [35,36], or of reaction-field corrections [37–41], may eliminate some of these artifacts, but these methods nevertheless retain, and sometimes amplify, some of the undesirable effects of abrupt truncation [30,36,42–44]. On the other hand, the simulation of solvated (bio-)molecules using Ewald summation [6–8] or related, but computationally less expensive methods, such as the particle–particle particle mesh ($P_3M$ [9–11]), particle–mesh Ewald (PME [12–14]) or fast multipole (FMM [15–17]) methods, has led to stable trajectories in cases where cutoff-based methods have failed to do so [31–33,45,46]. For this reason, Ewald and related methods are nowadays routinely used for the explicit-solvent simulation of proteins [46] and nucleic acids (DNA [47–51] and RNA [52,53]) in solution, and may completely superseed the use of cutoff truncation in the near future.

Although the stability of a trajectory is a necessary condition for studying equilibrium observables of a molecular system, it is not a sufficient one to guarantee their correctness. The use of lattice summation methods implies that periodicity in a system simulated under periodic boundary conditions is considered to be an intrinsic property of this system. We refer to this choice as Ewald boundary conditions (EWBC). There are a number of reasons to expect that the use of EWBC for simulating solutions may lead to undesirable side effects. First, a solute is automatically present, under EWBC, at a finite and often large concentration. For example, a single solute molecule of charge $z = -8\ e$ (e.g. DNA tetranucleotide) surrounded by 1000 water molecules is formally present at a 0.056 $m$ (molal) concentration, defining a solution of 3.6 $m$ ionic strength. This system will probably behave neither like an ideal solution, nor like a solution at this same concentration, because the solute molecule and its periodic replicas cannot move with respect to one another. Second, the interaction energy under EWBC is sensitive to the orientation of the solute molecule in the central unit cell [54]. Third, charges at specific distances do not exert forces on each other (e.g. two charges at a distance $L/2$ along a line parallel to an edge of length $L$ of a cubic unit cell). Finally, when a non-neutral solute is considered, the use of EWBC implicitly introduces a homogeneous background charge that neutralizes the unit cell. This charge density will not model realistically the charge density arising from a counter-ion atmosphere, because (i) it overlaps with solute atoms; (ii) it is independent of the distance to the surface of the solute molecule; and (iii) it completely neutralizes the solute charge within an arbitrary volume of solution, the volume of the unit cell.

Artifacts linked with the use of EWBC to calculate free energies of ionic hydration are well understood [55–58], and appear in the form of a

systematic free energy shift linked with the Wigner self-energy [55,59–61]. Given the unit cell size, ionic radius and solvent permittivity, this shift can be calculated analytically based on continuum electrostatics [57,58]. A similar shift in the free energy is also observed in potentials of mean force (PMFs) for ion–ion interactions calculated under EWBC [62]. However, it essentially disappears when the Wigner self-energy is added to the calculated PMFs [58]. Molecular dynamics (MD) simulations [26,28,30], as well as continuum electrostatics calculations [58] indicate that the periodicity-induced perturbation of PMFs for ion–ion interaction is small for small monovalent ions in large enough unit cells surrounded by a solvent of high dielectric permittivity.

Other possible artifacts linked with the use of EWBC are still poorly characterized. A study of the dependence of the potential energy of model solutes (dipole, quadrupole and small protein) on their orientation within the unit cell indicated that Ewald rotational artifacts are negligible when solvents of high permittivities are considered [54]. However, this conclusion relies on the approximation that the periodicity-induced perturbation of the Coulomb interaction, which is not negligible, is directly scaled by the permittivity of the solvent due to dielectric screening. As we show below, this may not be correct for systems involving low-dielectric cavities of a non-negligible size. Finally, a comparison of three 1.5-ns explicit-solvent simulations of a DNA dodecamer using the PME method and three different unit cell sizes has been reported [63]. The root-mean-square deviations from the crystallographic structure and the DNA curvature were monitored, and no significant unit cell size dependence of these properties was observed. This result may indicate the absence of artifacts linked with EWBC in this specific system, but may also be due to a poor sensitivity of the two selected observables on the electrostatic interaction scheme, or to their slow convergence. Clearly, selecting sensitive and well-converged observables to assess the system-size dependence of simulations under EWBC is a difficult problem.

Ideally, one would like to perform a direct comparison between explicit-solvent simulations under non-periodic boundary conditions (NPBC) and EWBC. This is impossible since an explicit-solvent system under NPBC is infinite, unless other critical approximations are made (fixed boundary conditions or truncated electrostatic interactions). However, as described in a previous study [58], this comparison is possible if an implicit representation of the solvent is chosen (continuum electrostatics). Assuming that observations made using this implicit-solvent model are relevant (at least qualitatively) for simulations using explicit-solvent molecules, this method allows to investigate specifically the perturbation induced by artificial periodicity in (bio-)molecular simulations under EWBC. In the previous study, we showed that the effect of artificial periodicity on ion solvation and ion–ion interactions may be important when the solvent is of low permittivity, or when the ratio of the ion size to the unit cell size is large. Although both conditions are generally satisfied during simulations of small ions in water, biomolecules define larger low-dielectric cavities, and the second condition may no more be fulfilled. Consequently, artificial periodicity may significantly perturb the PMFs corresponding to conformational equilibria of biomolecules. To investigate this effect, we perform continuum electrostatic calculations on single conformations of biomolecules. Conformations are either selected along a simple conformational pathway, or taken from an MD simulation. Three model systems and conformational pathways are discussed: polyalanine oligopeptides (PMF for unfolding), a double-stranded DNA tetranucleotide (PMF for separating the two strands), and the small hyperthermophilic protein Sac7d from *Sulfolobus acidocaldaricus* [64–67] (conformations from an MD simulation).

## 2. Theory

Using a continuum representation of the solvent, the free energy of a solute–solvent system may be partitioned into a sum of a non-polar contribution, corresponding to the work required for creating the solute cavity in the solvent in the

absence of solute charges (including 'hydrophobic' and dispersion interactions), and an electrostatic contribution, corresponding to the work required for reversibly charging the solute atoms. Since the non-polar contribution is dominated by short-range (surface) effects, we assume that the periodicity-induced perturbation of this contribution is negligible, and will focus on the influence of artificial periodicity on the electrostatic contribution alone.

Under NPBC, the basic electrostatic entity is the point charge. Under EWBC, however, the application of the Poisson equation and the periodicity requirement for the electrostatic field impose the electroneutrality of the unit cell [58]. We thus consider that the basic electrostatic entity under EWBC is not the point charge, but the point charge plus homogeneous neutralizing background charge density (C + B charge). Unlike the point charge, the C + B charge possesses a self-energy [55–61]. With this definition, and as illustrated in Fig. 1, the electrostatic contribution to the free energy of a solvated solute under NPBC and EWBC, can be further partitioned into two and three terms, respectively. In practice, the solute is defined as a low-dielectric cavity of relative permittivity $\epsilon_i$, immersed in a solvent of higher permittivity $\epsilon_s$. The Coulomb term corresponds to interactions in a homogeneous medium of permittivity $\epsilon_i$ (when $\epsilon_i \neq 1$, the notation $G_{Cb}$ might be more appropriate than $E_{Cb}$). The solvation term corresponds to the work required for changing the permittivity outside the solute from $\epsilon_i$ to $\epsilon_s$. The self-energy term under EWBC corresponds to the sum of the self-energies of all solute C + B charges.

The perturbation of the electrostatic free energy induced by artificial periodicity can then be quantified as

$$\begin{aligned}\Delta\Delta G_{el} &= [\Delta G_{el}]_P - [\Delta G_{el}]_{NP} \\ &= \left([E_{Cb}]_P + [\Delta G_{self}]_P + [\Delta G_{solv}]_P\right) \\ &\quad - \left([E_{Cb}]_{NP} + [\Delta G_{solv}]_{NP}\right)\end{aligned} \tag{1}$$

We further define the periodicity-induced perturbations in the Coulomb and solvation contributions as

$$\Delta E_{Cb} = [E_{Cb}]_P - [E_{Cb}]_{NP} \quad \text{and}$$

$$\Delta\Delta G_{solv} = [\Delta G_{solv}]_P - [\Delta G_{solv}]_{NP} \tag{2}$$

so that $\Delta\Delta G_{el} = \Delta E_{Cb} + \Delta\Delta G_{solv} + [\Delta G_{self}]_P$. The term $[\Delta G_{self}]_P$ has been singled out in Fig. 1 because it behaves in some respect like a Coulomb term and in some respect like a solvation term. For neutral systems, it is reasonable to associate this term with the Coulomb contribution, since it is also present in the absence of solvent. For non-neutral systems, however, the periodic replicas of the solute and the homogeneous background charge may be viewed as forming a counter-ion atmosphere for the central solute molecule [58]. In this case, it may be more physically meaningful to associate it with the solvation term. For the ease of presentation of the results $[\Delta G_{self}]_P$ will be associated with either the Coulomb or the solvation contribution. We define the primed quantities $[E'_{Cb}]_P$, $[\Delta G'_{solv}]_P$, $\Delta E'_{Cb}$, and $\Delta\Delta G'_{solv}$ as the corresponding quantities from Eqs. (1) and (2), increased by $[\Delta G_{self}]_P$.

In the following paragraphs, we briefly state the equations allowing us to calculate the five (free) energy contributions of Eq. (1), for a solute bearing $N_{at}$ atomic point charges $\{q_i\}$ at locations $\{\mathbf{r}_i\}$. The solvation free energies are obtained from a finite-difference solution to the Poisson equation. Rectangular Dirichlet boundary conditions (potential specified on the surface of the unit cell) are used to mimic NPBC, whereas rectangular periodic boundary conditions (periodic potential and dielectric permittivity) represent EWBC. The Coulomb energies are estimated by pairwise Coulomb summation under NPBC, and Ewald summation under EWBC. More details about the derivation of the equations and their numerical solution, as well as the possible use of the linearized Poisson–Boltzmann equation to include implicit counter-ions in the calculations, are presented elsewhere [58]. The solvation contribution under NPBC is calculated as

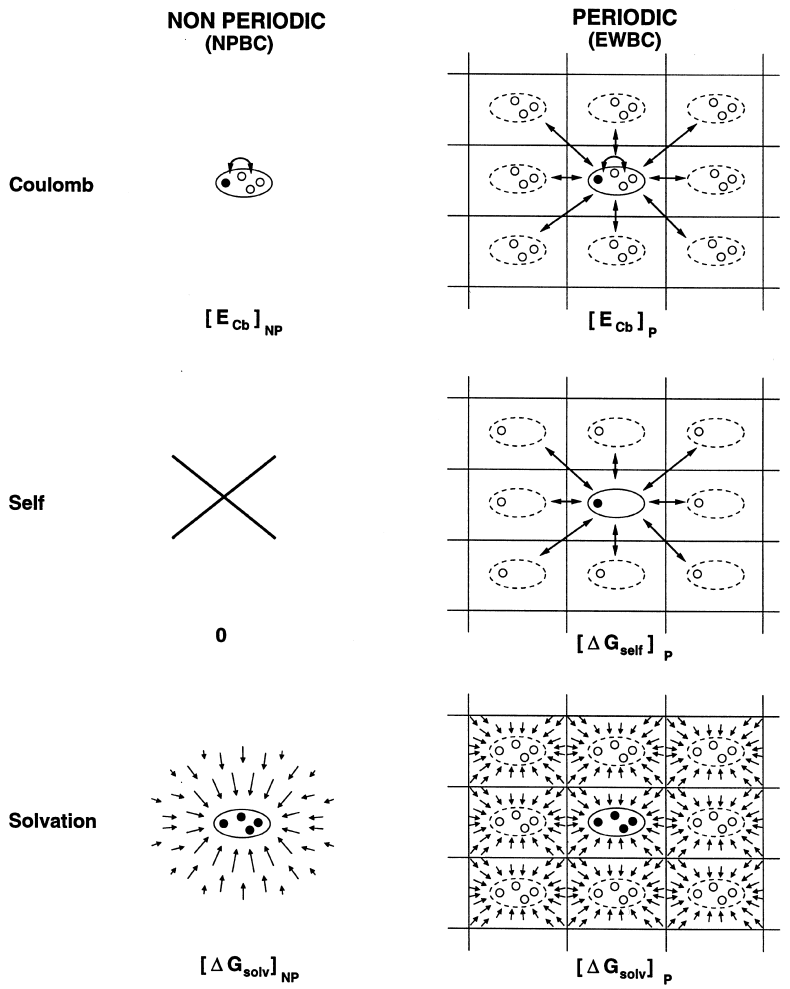


Fig. 1. Contributions to the electrostatic free energy of a solvated solute. The different contributions are illustrated for a solute containing four charges, under non-periodic (NPBC) or Ewald (EWBC) boundary conditions. Circles represent charges (NPBC) or C + B charges (EWBC). Double-ended arrows in the four upper diagrams represent sets of Coulomb interactions between a reference charge (●) and other charges (○). $[E_{Cb}]_{NP}$ is the sum of Coulomb interactions between a given solute charge (●) and all other solute charges (○). $[E_{Cb}]_P$ is the sum of Coulomb interactions between a given C + B charge in the central solute (●) and all other C + B charges in the central solute plus their periodic copies (○). $[\Delta G_{self}]_P$ is the sum of the self-energies of C + B charges in the central solute (●). The self-energy of a C + B charge corresponds to the work for reversibly charging the central charge in the potential created by its periodic copies (○) and the homogeneous background charge (Wigner potential [55,59–61]). Arrows in the two lower diagrams represent solvent dipoles. $\Delta G_{solv}$ represents the interaction between charges in the central solute molecule (●) and the solvent dipoles (arrows). In $[\Delta G_{solv}]_{NP}$, the solvent is polarized by charges of the single solute molecule (●). In $[\Delta G_{solv}]_P$, the solvent is polarized by the C + B charges in the central solute molecule (●) and their replicas (○).

$$[\Delta G_{solv}]_{NP} = [G]_{NP}(\epsilon_i, \epsilon_s) - [G]_{NP}(\epsilon_i, \epsilon_i)$$

with

$$[G]_{NP} = \frac{1}{2}\sum_{i}^{N_{at}} q_i \Phi_{NP}(\mathbf{r}_i) \qquad (3)$$

Here, $\Phi_{NP}(\mathbf{r})$ is the (non-periodic) electrostatic potential corresponding to specific values of $\epsilon_i$ and $\epsilon_s$. This potential is a solution of the Poisson equation

$$-\epsilon_o \nabla \cdot [\epsilon(\mathbf{r}) \nabla \Phi(\mathbf{r})] = \rho(\mathbf{r}) \qquad (4)$$

where $\epsilon(\mathbf{r})$ is the heterogeneous relative dielectric permittivity (defined by $\epsilon_i$ and $\epsilon_s$, respectively, inside and outside the solute), and $\rho(\mathbf{r})$ the charge density originating from the solute charges. As described elsewhere [58,68], Eq. (4) may be discretized on a grid spanning the unit cell using a finite-difference scheme, and solved for the gridded electrostatic potential, from which $\Phi_{NP}(\mathbf{r})$ is interpolated. This solution requires knowledge of the boundary potential, $\Phi_b(\mathbf{r})$, at the surface of the unit cell. This potential is approximated by the Coulomb expression for a medium of homogeneous permittivity $\epsilon_s$

$$\Phi_b(\mathbf{r}) = \sum_{i=1}^{N_{at}} \frac{q_i}{4\pi\epsilon_o\epsilon_s} \frac{1}{\|\mathbf{r}-\mathbf{r}_i\|} \tag{5}$$

If the unit cell is large enough, so that all solute atoms are at distances from the surface of the unit cell which are large compared to their atomic radii, this finite system will mimic an infinite system under NPBC with a reasonable accuracy. The solvation contribution under EWBC is calculated as

$$[\Delta G_{solv}]_P = [G]_P(\epsilon_i,\epsilon_s) - [G]_P(\epsilon_i,\epsilon_i)$$

with

$$[G]_P = \frac{1}{2}\sum_i^{N_{at}} q_i[\Phi_P(\mathbf{r}_i) - \langle\Phi_P(\mathbf{r})\rangle_V] \tag{6}$$

where $\langle ... \rangle_V$ denotes averaging over the volume of the unit cell. Here, $\Phi_P(\mathbf{r})$ is the periodic electrostatic potential corresponding to specific values of $\epsilon_i$ and $\epsilon_s$. This potential is a solution of the Poisson equation under EWBC

$$-\epsilon_o\nabla\cdot[\epsilon(\mathbf{r})\nabla\Phi(\mathbf{r})] = \rho(\mathbf{r}) - \langle\rho(\mathbf{r})\rangle_V \tag{7}$$

As described in a previous article [58], Eq. (7) may be discretized on a grid spanning the periodic unit cell using a finite-difference scheme, and solved under periodic boundary conditions for the gridded electrostatic potential, from which $\Phi_P(\mathbf{r})$ is interpolated.

The Coulomb energy under NPBC is given by Coulomb's law

$$[E_{Cb}]_{NP} = \frac{1}{4\pi\epsilon_o\epsilon_i}\frac{1}{2}\sum_{i=1}^{N_{at}}\sum_{j=1,j\neq i}^{N_{at}}{}' \frac{q_iq_j}{r_{ij}} \tag{8}$$

The prime after the summation sign indicates that pairs of atoms which are excluded neighbours (usually first and second covalent neighbours) are omitted. Under EWBC, the interaction energy is calculated by Ewald summation [6–8]. In the present study, we use a Gaussian charge shaping function of inverse width $\alpha$, together with so-called 'tinfoil' boundary conditions (zero potential at the surface of the infinite periodic system). These choices result in the two following terms [58]: a pairwise interaction energy term

$$[E_{Cb}]_P = \frac{1}{\epsilon_i}\frac{1}{2}\sum_{i=1}^{N_{at}}\sum_{j=1,j\neq i}^{N_{at}} q_iq_j\psi(\mathbf{r}_{ij}) \tag{9}$$

with $\mathbf{r}_{ij} = \mathbf{r}_j - \mathbf{r}_i$, and a self-energy term

$$[\Delta G_{self}]_P = \frac{1}{4\pi\epsilon_o\epsilon_i}\frac{A(L_x,L_y,L_z)}{2}\sum_{i=1}^{N_{at}} q_i^2 \tag{10}$$

The function $\psi(\mathbf{r})$ is given by

$$\psi(\mathbf{r}) = \frac{1}{4\pi\epsilon_o}\left[\sum_{l=-\infty}^{\infty}{}' \frac{\mathrm{erfc}(\alpha\|\mathbf{r}+\underline{\mathbf{L}}\mathbf{l}\|)}{\|\mathbf{r}+\underline{\mathbf{L}}\mathbf{l}\|} + \frac{4\pi}{V}\sum_{\mathbf{l}=-\infty,\mathbf{l}\neq\mathbf{0}}^{\infty}\frac{\mathrm{e}^{-k^2/(4\alpha^2)}}{k^2}\cos\mathbf{kr} - \frac{\pi}{V\alpha^2}\right] \tag{11}$$

where $\underline{\mathbf{L}}$ is a diagonal matrix with elements $L_x$, $L_y$ and $L_z$, the dimensions of the rectangular unit cell, $\mathbf{l}$ is a vector with integer components, $\mathbf{k} = 2\pi\underline{\mathbf{L}}^{-1}\mathbf{l}$, and erfc is the complementary error function. The prime after the summation sign indicates that when $\mathbf{l}=\mathbf{0}$ and for pairs of atoms which are excluded neighbours, erfc should be substituted by erfc $-1$. When $\alpha$ is large enough so that $r^{-1}$ erfc$(\alpha r)$ is a short-ranged function, the sum in the first term of Eq. (11) may be truncated to the $\mathbf{l}=\mathbf{0}$ term, in which case, $\mathbf{r}_{ij}$ in

Eq. (9) should be the minimum-image vector between charges $i$ and $j$. The constant $A(L_x,L_y,L_z)$, which defines the Wigner potential, must be evaluated numerically. In the case of a cubic unit cell ($L_x = L_y = L_z = L$) we have [55–61]

$$A = \frac{\xi_{EW}}{L} \quad \text{with} \quad \xi_{EW} \approx -2.837297 \tag{12}$$

We note finally that Eqs. (8) and (9) do not exactly describe the work required for assembling the solute charges from infinite separation, due to the absence of interactions between excluded neighbours. However, if the distances between excluded neighbours are fixed, these expressions are correct within a (force-field dependent) constant. Since this constant is identical under NPBC and EWBC, it can safely be ignored in the comparison between Coulomb energies corresponding to the two types of boundary conditions.

## 3. Molecular model and computational procedures

Coordinates for polyalanine oligopeptides of $N$-residue length ($N = 2$, 4, 6, 8 or 10) were generated using the program CHARMm [69]. The conformation of the chain is controlled by the dimensionless parameter $\lambda$, which defines the backbone $\Phi$ and $\psi$ angles of all residues through

$$\Phi(\lambda) = -57°(1-\lambda) - 180°\lambda \text{ and}$$
$$\psi(\lambda) = -47°(1-\lambda) - 180°\lambda \tag{13}$$

The value $\lambda = 0$ corresponds to the $\alpha$-helical conformation, and $\lambda = 1$ to the extended, all-trans conformation. $\lambda$ is varied from 0 to 1 by increments of 0.05. Other internal coordinates (bond lengths, bond angles, and improper dihedral angles) are fixed to standard values [69]. Results are reported as a function of the end-to-end distance $e$, measured between $\mathrm{Ala}_1$ ($\mathrm{N}_{NH}$) and $\mathrm{Ala}_N$ ($\mathrm{C}_{CO}$). Two charge states of the chain termini are considered: neutral ($\mathrm{NH}_2$– at the N-terminus and –COOH at the C-terminus), or charged ($\mathrm{NH}_3^+$– at the N-terminus and $-\mathrm{COO}^-$ at the C-terminus). Conformations corresponding to $\lambda = 0$ and 1 for the octapeptide ($N = 8$) with charged termini are represented in Fig. 2a,b.

Initial coordinates for the double-stranded DNA tetranucleotide 3′-TCGA-5′ were taken from the crystallographic coordinates of the double-stranded decanucleotide 3′-CTC[TCGA]-GAG-5′ [70], entry 196D of the Protein Data Bank. The DNA conformation is controlled by a translation distance $d$ between the two strands, so that $d = 0$ nm corresponds to the crystal structure. The distance $d$ is increased from 0 to 1.5 nm by increments of 0.02 nm. Other internal coordinates are fixed to values derived from the crystal structure. Two charge states of the system are

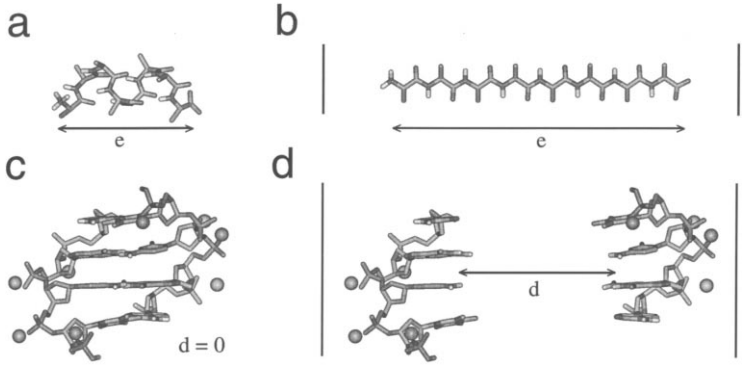


Fig. 2. Conformations of the polyalanine oligopeptides and DNA tetranucleotide. (a,b) Conformations of the octapeptide ($N = 8$) with charged termini corresponding to $\lambda = 0.0$ (a) and 1.0 (b) in Eq. (13); the corresponding end-to-end distances $e$ are 1.3 and 2.8 nm; (c,d) conformations of the double-stranded DNA tetranucleotide (3′-TCGA-5′) corresponding to $d = 0.0$ nm (c) and $d = 1.5$ nm (d); explicit $Na^+$ counter-ions (only included in some calculations) are represented as balls. Vertical lines in (b) and (d) indicate the nearest unit cell walls in the direction of elongation, for a cubic unit cell of edge $L = 4$ nm.

considered: charged (DNA of charge $-8$ $e$, no explicit counter-ions), or neutral (eight $Na^+$ counter-ions included). In the latter case, the counter-ions were placed at the midpoint between the two backbone phosphate oxygens forming no bonds with a carbon, and their coordinates optimized by energy minimization in vacuum, keeping other atoms fixed. Configurations corresponding to $d = 0$ and 1.5 nm are displayed in Fig. 2c,d for the system including explicit counter-ions.

Sac7d is a small (66 residues, among which 32 charged) hyperthermophilic protein ($T_m \approx 100°C$) from the organism *Sulfolobus acidocaldaricus* [64–66]. We carried out [67] a 0.9-ns MD simulation of the protein at 550 K, using the GROMOS96 program and force-field [71] together with the $P_3M$ method [9–11]. The simulation was performed in a rectangular unit cell containing the protein and 3956 SPC water molecules in the absence of counter-ions (total system charge $+6$ $e$). As evidenced by the time evolution of the radius of gyration, root-mean-square deviation from the NMR structure, and secondary structure content [67], this simulation did not achieve unfolding of the protein. This result is in contrast with other protein simulations at similar temperatures and of similar lengths, but using cutoff truncation of the electrostatic interactions [72–75]. To investigate whether the perturbation imposed by artificial periodicity under EWBC may be responsible for the unexpected stability of the protein during this simulation, the continuum analysis presented here was applied to 180 configurations taken from the simulated trajectory at intervals of 5 ps.

For the three systems, the solvation free energies under NPBC Eq. (3), or EWBC Eq. (6), were calculated using a modified version of the UHBD program [68]. A grid spacing $g = 0.05$ nm was selected. For the oligopeptides and the tetranucleotide, calculations under EWBC were performed using a cubic unit cell of edge $L = 4$ nm. For Sac7d, the unit cell dimensions under EWBC were those used during the MD simulation, $4.7 \times 4.9 \times 5.6$ nm. Under NPBC, the edge lengths were increased by a distance $D = 2$ nm with respect to the EWBC value, in order to increase the distances between the solute atoms and the surface of the unit cell, and Eq. (5) was used to define the potential on the surface of the enlarged unit cell. For the oligopeptides and the tetranucleotide, the three principal axes of the solute were aligned with the Cartesian axes of the unit cell prior to calculation. This was not done for the Sac7d configurations. Solute cavities were defined as the contact and reentrant surface obtained by rolling a probe of 0.14 nm radius over the molecule. For the oligopeptides and the tetranucleotide, the atomic radii and charges were taken from the commercial version of the CHARMm(22) force field [69]. For Sac7d, the GROMOS96 atomic charges and radii [71] were employed for compatibility with the MD simulation. The solute and solvent permittivities were set to $\epsilon_i = 1$ and $\epsilon_s = 78$ (water), respectively, and the temperature to $T = 300$ K.

The Coulomb interaction energies under NPBC Eq. (8), and EWBC Eq. (9), were calculated using a modified version of the GROMOS96 program [71], using either CHARMm(22) (oligopeptides, tetranucleotide) or GROMOS96 (Sac7d) charges. Under EWBC (Ewald summation), a Gaussian shaping function of inverse width $\alpha = 4$ nm$^{-1}$ was used, together with a real-space cutoff $R_c = 1$ nm and $\boldsymbol{l}$-vector components ranging from $-l_{max}$ to $l_{max}$ and overall norm inferior to $l_{max}^2$, with $l_{max} = 50$. The sensitivity of the results on the specific choice of $D$, $g$, $\alpha$, $R_c$ and $l_{max}$ was tested, and small changes in these parameters did not alter significantly the calculated (free) energies.

## 4. Results

### 4.1. Polyalanine oligopeptides with neutral termini

The Coulomb and solvation contributions to the electrostatic free energy for the polyalanine oligopeptides with neutral termini, under NPBC and EWBC, are displayed in Fig. 3a as a function of the end-to-end distance $e$. The contribution $[\Delta G_{self}]_P$ to $[E'_{Cb}]_P$ is a constant and evaluates to $-103.0$, $-191.2$, $-279.4$, $-367.6$, and $-455.8$ kJ/mol for $N = 2$, 4, 6, 8, and 10, respectively. The curves corresponding to $[E_{Cb}]_{NP}$ and $[E'_{Cb}]_P$, as well as those corresponding to $[\Delta G_{solv}]_{NP}$ and

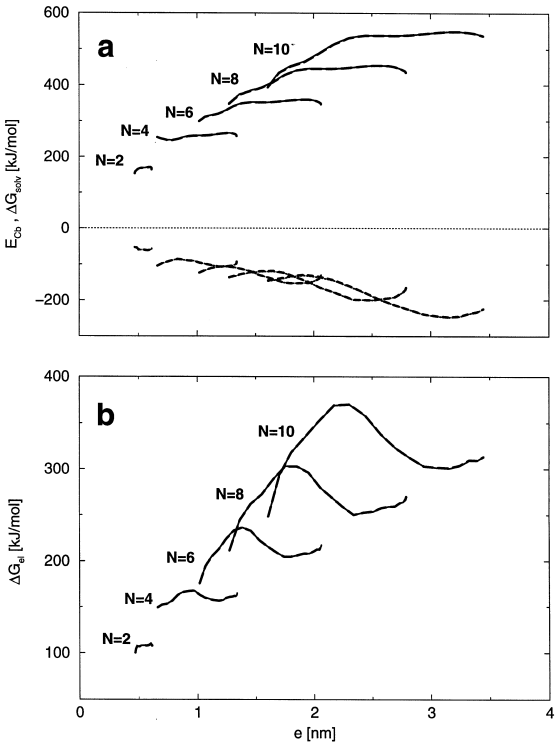


Fig. 3. Electrostatic contributions to the PMF for unfolding oligopeptides with neutral termini. Coulomb and solvation contributions to the electrostatic free energy (a), as well as their sum (b), under NPBC and EWBC, are displayed as a function of the end-to-end distance $e$ for polyalanine oligopeptides with $N$ residues ($N = 2$, 4, 6, 8 or 10). The solute and solvent relative permittivities are $\epsilon_i = 1$ and $\epsilon_s = 78$, respectively. Under EWBC, the periodic unit cell is a cube of edge $L = 4$ nm, and the principal axes of the oligopeptide are aligned with the edges of the cube. (a) Coulomb and solvation contributions: $[E_{Cb}]_{NP}$ (———) from Eq. (8), $[E'_{Cb}]_P \equiv [E_{Cb}]_P + [\Delta G_{self}]_P$ (— — —) from Eqs. (9) and (10), $[\Delta G_{solv}]_{NP}$ (.....) from Eq. (3), and $[\Delta G_{solv}]_P$ (-----) from Eq. (6); (b) total electrostatic free energy: $[\Delta G_{el}]_{NP}$ (———) and $[\Delta G_{el}]_P$ (— — —), see Eq. (1). Curves corresponding to NPBC and EWBC are nearly indistinguishable on the scale of the graphs.

$[\Delta G_{solv}]_P$, are indistinguishable on the scale of the graph. The Coulomb contribution increases with increasing $e$, due to the disruption of hydrogen bonds between backbone amide groups. The sign of this contribution (positive in the present case) is force-field dependent and irrelevant (see Section 2). The solvation contribution is always negative, since electrostatic solvation is a favorable process. After a slight initial increase, the curves decrease with increasing $e$ due to the exposure of polar backbone amide groups to the solvent. Finally, the curves increase slightly again for highly extended conformations.

The curves representing the sum of the two contributions, i.e. the total electrostatic contribution to the PMF, are displayed in Fig. 3b. Here again, curves corresponding to NPBC and EWBC do not significantly differ. Under NPBC, the $\alpha$-helical conformations are separated from more extended conformations by barriers of 9.2, 18.2, 60.1, 91.2, and 121.7 kJ/mol for $N = 2$, 4, 6, 8, and 10, respectively, as measured from the $\alpha$-helical conformation to the maximum of the PMF. These values are increased by 0.1–0.2 kJ/mol under EWBC. Under NPBC, the $\alpha$-helical conformations are favored electrostatically with respect to extended conformations by 6.5, 7.1, 28.6, 38.6, and 52.3 kJ/mol for $N = 2$, 4, 6, 8, and 10, respectively, as measured from the $\alpha$-helical conformation to the other minimum of the PMF. These values are increased by 0.2–0.4 kJ/mol under EWBC. That the $\alpha$-helical conformation is favored electrostatically does not mean, however, that it is actually more stable, since the shape of the overall PMF depends on three other contributions: (i) covalent interactions, especially terms arising from torsional dihedral angles; (ii) non-polar interactions, including solute–solute and solute–solvent van der Waals interactions, and a cavity or 'hydrophobic' term; and (iii) a contribution arising from the conformational entropy of the chain, which depends on the average of the Boltzmann factor over all conformations compatible with a given value of $e$. Whereas the first contribution is probably minor, the second contribution is likely to be large. Below the value of $e$ corresponding to the $\alpha$-helical conformation, the solute–solute van der Waals term will increase sharply with decreasing $e$, balancing the decrease in the electrostatic free energy with decreasing $e$. The cavity term will favor the more compact $\alpha$-helical conformation. Finally, the entropic contribution is likely to disfavor both the $\alpha$-helical and all-trans conformations with respect to intermediate ones. This entropic contribution will also drastically reduce the unrealistically high

barriers displayed by the electrostatic PMFs for the unfolding of the helices. In other words, the one-parameter unfolding pathways described by Eq. (13) are too simplistic to account correctly for the true free energy barriers.

Although the electrostatic PMFs displayed in Fig. 3b should not be overinterpreted, they are probably sufficient to investigate qualitatively the effect of artificial periodicity on the conformational equilibrium. The curves representing the periodicity-induced perturbation of the Coulomb and solvation contributions are displayed in Fig. 4a. The perturbations are small in magnitude (at most $\pm 2.3$ kJ/mol for the $\alpha$-helical conformation of the decapeptide) compared to the contributions themselves. The shift caused by artificial periodicity in the Coulomb contribution is always negative. It is caused by the favorable interaction between the dipole of the oligopeptide in the central unit cell and the aligned dipoles of its periodic replicas. Note that the interaction between a dipole in the central unit cell and its aligned replica in an adjacent unit cell will be stabilizing only for cells which are located in the direction of the dipole. However, since oligopeptides are very elongated in the direction of the dipole, the stabilizing interactions will dominate. Since this effect is correlated with the size of the dipole moment (Fig. 4a, inset), its magnitude decreases with increasing $e$ to reach a value close to zero for the all-trans conformation. The shift in the solvation contribution caused by artificial periodicity is always positive. It is caused by the perturbation of the solvent by the periodic replicas of the oligopeptide, which renders the solvent less available for the solvation of the central oligopeptide, see Fig. 1. Since the solvation of a dipole in a cavity is related to the square of the dipole moment [76], this effect is correlated with the size of the dipole moment of the oligopeptide, and decreases with increasing $e$ to reach a value close to zero for the all-trans conformation. The decrease is monotonic except for the decapeptide ($N = 10$), where we observe a peak at high extension. This peak may be due to the increase in the dipole moment observed for the most extended conformations of long oligopeptides (Fig. 4a, inset). Alternatively, it may correlate with the close

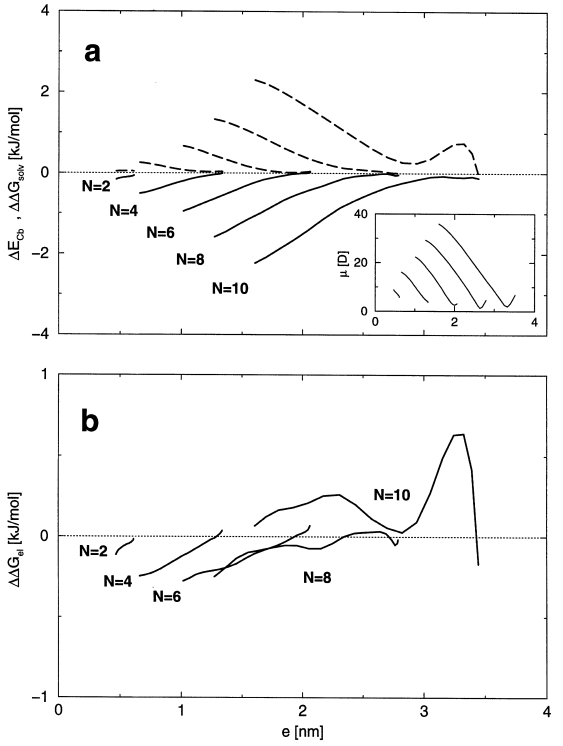


Fig. 4. Periodicity-induced perturbation of the PMF for unfolding oligopeptides with neutral termini. The periodicity-induced perturbations of the Coulomb and solvation contributions (a), as well as of their sum (b), are displayed as a function of the end-to-end distance $e$ for oligopeptides with $N$ residues ($N = 2$, 4, 6, 8 or 10). See legend of Fig. 3. (a) Perturbation of the Coulomb contribution, $\Delta E'_{Cb} \equiv \Delta E_{Cb} + [\Delta G_{self}]_P$ (———), and of the solvation contribution, $\Delta\Delta G_{solv}$ (— — —), see Eq. (2); inset: overall dipole moment of the oligopeptides as a function of $e$ for (left to right) $N = 2$, 4, 6, 8 and 10; (b) perturbation of the total electrostatic free energy, $\Delta\Delta G_{el}$, from Eq. (1).

proximity ($< 1$ nm) between the termini of the central oligopeptide and the opposite termini of oligopeptides in adjacent unit cells.

The sum of the periodicity-induced shifts in the Coulomb and solvation contributions, $\Delta\Delta G_{el}$, is displayed in Fig. 4b. The two opposite effects, already small individually, significantly cancel each other resulting in an overall perturbation of very small magnitude (always below 0.3 kJ/mol, except for $N = 10$). For $N = 2$–8, the perturbation in the Coulomb contribution slightly dominates, and artificial periodicity results in a weak

stabilization of the $\alpha$-helical conformation with respect to more extended ones. For $N = 10$, the solvation effect dominates for the most extended conformations and a peak is observed at $e = 3.3$ nm, as was the case in the perturbation of the solvation contribution (Fig. 4a).

### 4.2. Polyalanine oligopeptides with charged termini

The Coulomb and solvation contributions to the electrostatic free energy for the polyalanine oligopeptides with charged termini, under NPBC and EWBC, are displayed in Fig. 5a. The contribution $[\Delta G_{self}]_P$ to $[E'_{Cb}]_P$ is a constant and evaluates to $-102.2$, $-190.4$, $-278.6$, $-366.8$, and $-455.0$ kJ/mol for $N = 2$, 4, 6, 8 and 10, respectively. In contrast to the case of oligopeptides with neutral termini (Fig. 3a), the curves corresponding to NPBC and EWBC now differ significantly on the scale of the graph for $N \geq 8$. The Coulomb contributions, $[E_{Cb}]_{NP}$ and $[E'_{Cb}]_P$, decrease with increasing $e$. Oligopeptides with charged termini are destabilized by the unfavorable interaction between the dipole created by backbone amide groups and the charges at the chain termini. The magnitude of this interaction is correlated with the size of the backbone dipole moment (see Fig. 4a, inset) and thus decreases with increasing $e$. The slope of the curve is more negative under EWBC. The solvation contributions, $[\Delta G_{solv}]_{NP}$ and $[\Delta G_{solv}]_P$, are negative and increase with $e$, the slope of the curve being more positive under EWBC.

Curves representing the total electrostatic contribution to the PMF are displayed in Fig. 5b. Under NPBC, the $\alpha$-helical conformations are separated from extended conformations by barriers of 6.8, 7.3, 12.5, 40.1, and 69.7 kJ/mol for $N = 2$, 4, 6, 8 and 10, respectively, as measured from the $\alpha$-helical conformation to the maximum of the PMF. Extended conformations are favored electrostatically with respect to $\alpha$-helical conformations by $-35.7$, $-21.3$, $-29.3$, $-26.9$, and $-16.3$ kJ/mol for $N = 2$, 4, 6, 8 and 10, respectively, as measured from the $\alpha$-helical conformation to the other minimum of the PMF. The electrostatic free energies of the $\alpha$-helical conformations are weakly affected by the introduction of periodicity. However, extended conformations have significantly higher electrostatic free energies under EWBC. Artificial periodicity increases the barriers by 0.0, 0.1, 0.1, 0.4, and 0.5 kJ/mol, and the free energy differences between extended and $\alpha$-helical conformations by 0.3, 0.6, 1.1, 1.1, and 3.6 kJ/mol for $N = 2$, 4, 6, 8 and 10, respectively. The magnitude of the perturbation is in no case strong enough to invert the relative electrostatic stabilities of the $\alpha$-helical and extended conformations when going from NPBC to EWBC. Note, however, that the overall PMF depends on additional covalent, non-polar and entropic con-

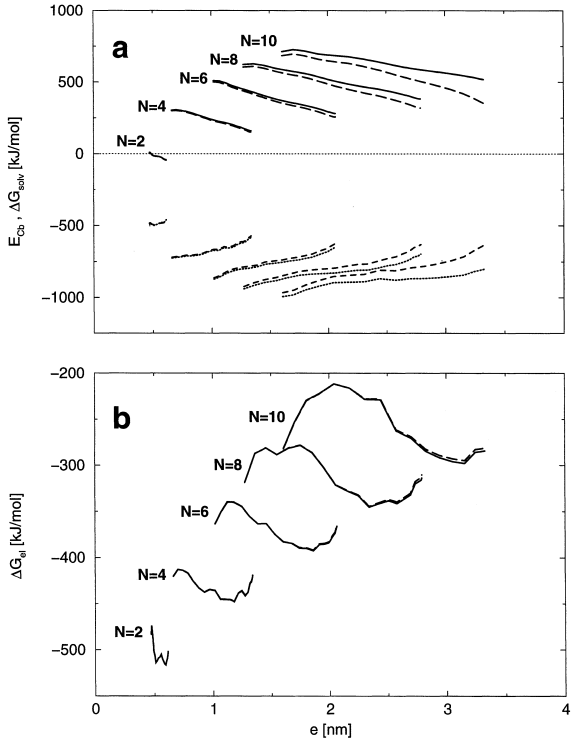


Fig. 5. Electrostatic contributions to the PMF for unfolding oligopeptides with charged termini. Coulomb and solvation contributions to the electrostatic free energy (a), as well as their sum (b), under NPBC and EWBC, are displayed as a function of the end-to-end distance $e$ for polyalanine oligopeptides with $N$ residues ($N = 2$, 4, 6, 8 or 10). See legend of Fig. 3. Curves corresponding to NPBC and EWBC can now be distinguished on the scale of the graphs (for $N \geq 8$).

tributions (see above), so that we cannot draw conclusions on which conformations will dominate in an MD simulation under EWBC.

To understand the causes of the periodicity-induced shifts observed in Fig. 5, the periodicity-induced perturbation of the Coulomb and solvation contributions are presented in Fig. 6a. The shift in the Coulomb contribution caused by artificial periodicity is in all cases negative. It decreases quasi-linearly in magnitude with increasing $e$, and is close to zero for the $\alpha$-helical conformation. This negative shift is due to the favorable interaction between the charged termini of the oligopeptide in the central unit cell and the oppositely charged termini of the oligopeptides in adjacent unit cells, an effect which is larger for extended conformations. An equally valid view is that the overall dipole moment, including contributions from the backbone amide groups and charged termini, is dominated by the latter contribution and thus increases with increasing $e$ (Fig. 6a, inset). Consequently, the favorable dipole–dipole interactions between the central dipole and dipoles in adjacent unit cells increase in magnitude with increasing $e$. The shift in the solvation contribution caused by artificial periodicity is in all cases positive, and increases steeply in magnitude with increasing $e$. Again, there are two alternative interpretations. First, the minimum image distance between positive and negative charges on opposite termini of the central chain and its periodic replicas decreases with increasing $e$, thereby reducing their solvation. Second, this shift may be viewed as a consequence of the perturbation of the solvent by the periodic replicas of the solute, which renders the solvent less available for the solvation of the central solute. As in the case of oligopeptides with neutral termini, the effect increases in magnitude with the size of the overall dipole moment. However, unlike in the former case, the overall dipole moment now increases with increasing $e$.

The sum of the periodicity-induced shifts in the Coulomb and solvation contributions, $\Delta\Delta G_{el}$, is displayed in Fig. 6b. The two opposite effects largely compensate each other, especially for the smallest oligopeptides ($N = 2$ or 4), and for the most compact conformations. However, for longer oligopeptides, the solvation effect dominates, and induces a strong stabilization of the $\alpha$-helical conformation with respect to more extended ones. This test system illustrates that the effect of the solvent cannot be reduced to a scaling of the perturbation of the Coulomb contribution by $\epsilon_s$. Evaluating the periodicity-induced perturbation in this way will generally lead to underestimating the effect [54]. To obtain a more accurate description, the perturbation of the solvation contribution needs to be calculated explicitly, as is done in the present study.

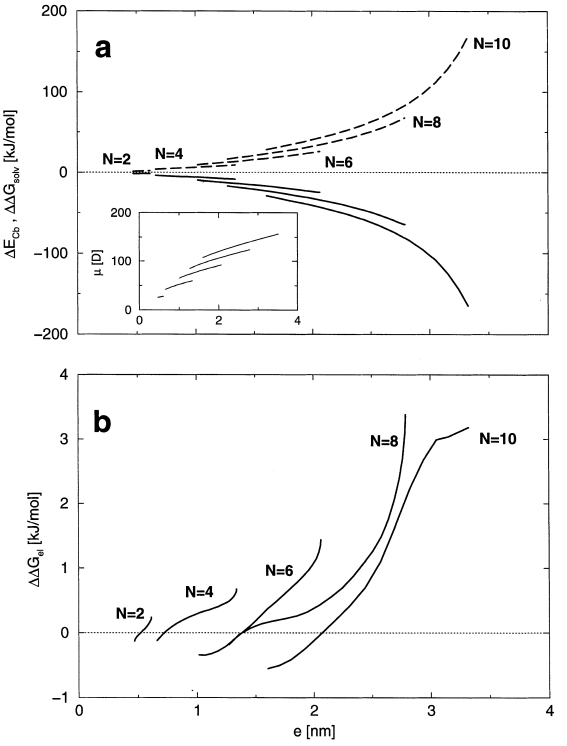


Fig. 6. Periodicity-induced perturbation of the PMF for unfolding oligopeptides with charged termini. The periodicity-induced perturbations of the Coulomb and solvation contributions (a), as well as of their sum (b), are displayed as a function of the end-to-end distance $e$ for oligopeptides with $N$ residues ($N = 2$, 4, 6, 8 or 10). See legend of Fig. 4. Inset in (a): overall dipole moment of the oligopeptides as a function of $e$ for (left to right) $N = 2$, 4, 6, 8 and 10. The contributions of backbone amide groups to this overall dipole moment are very similar to those displayed in the inset of Fig. 4a.

A relevant question at this point is: what is the minimal dimension of the unit cell required to render the periodicity-induced perturbation negligible? We address this question in the specific case of the octapeptide ($N = 8$). The periodicity-induced perturbation of the PMF, $\Delta\Delta G_{el}$, is displayed in Fig. 7 for four different unit cell sizes. As expected, the perturbation becomes less important when the box size increases. The differences in $\Delta\Delta G_{el}$ between the most extended conformation and the $\alpha$-helical conformation are 3.3, 1.1, 0.5, and 0.2 kJ/mol for $L = 4$, 5, 6 and 8 nm, respectively. This quantity varies with the unit cell size as $L^{-5}$, and a linear least-squares fit leads to a proportionality coefficient of 3254 kJ·nm$^5$/mol. Thus we estimate that boxes of edge larger than 4.3 or 7.3 nm are required in order to keep this difference below $k_BT$ or 0.1 $k_BT$, respectively.

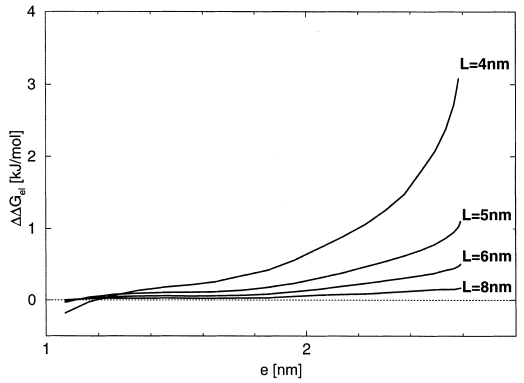


Fig. 7. Periodicity-induced perturbation of the PMF for unfolding an octapeptide with charged termini. The periodicity-induced perturbation of the PMF is displayed as a function of the end-to-end distance $e$ for four different sizes of the cubic unit cell. See legend of Fig. 6.

### 4.3. DNA tetranucleotide

The Coulomb contributions, under NPBC and EWBC, to the PMF for separating the two strands of the DNA tetranucleotide in the absence of counter-ions are displayed in Fig. 8a. Under NPBC, $[E_{Cb}]_{NP}$ increases with increasing $d$ for $d < 0.15$ nm, due to the disruption of hydrogen bonds between base pairs. Beyond this distance,

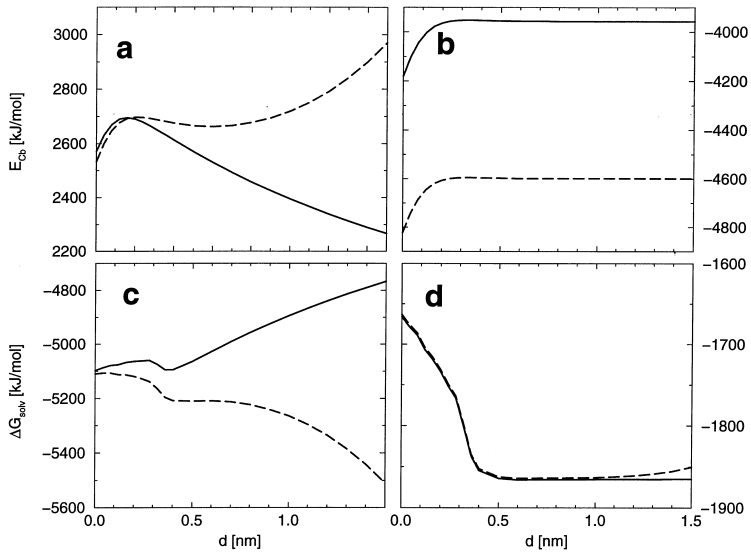


Fig. 8. Electrostatic contributions to the PMF for separating the strands of the DNA tetranucleotide. The Coulomb (a,b) and solvation (c,d) contributions to the electrostatic free energy are displayed as a function of the strand-to-strand distance $d$ (see Fig. 2) for the DNA tetranucleotide 3′-TCGA-5′, in the absence (a,c) or presence (b,d) of eight explicit $Na^+$ counter-ions. The solute and solvent relative permittivities are $\epsilon_i = 1$ and $\epsilon_s = 78$, respectively. Under EWBC, the periodic unit cell is a cube of edge $L = 4$ nm, and the principal axes of the tetranucleotide are aligned with the edges of the cube. (a,c) Coulomb contributions, $[E_{Cb}]_{NP}$ (——) from Eq. (8), and $[E_{Cb}]_P$ (— — —) from Eq. (9); (b,d) solvation contributions: $[\Delta G_{solv}]_{NP}$ (——) from Eq. (3) and $[\Delta G'_{solv}]_P \equiv [\Delta G_{solv}]_P + [\Delta G_{self}]_P$ (— — —) from Eqs. (6) and (10).

$[E_{Cb}]_{NP}$ is a decreasing function of $d$, due to the decreasing repulsion between the negatively-charged phosphate groups on the two DNA strands. Under EWBC, a similar initial increase in $[E_{Cb}]_P$ is observed for $d < 0.2$ nm, followed by a slight decrease between 0.2 and 0.5 nm. Beyond this distance, and in contrast to the NPBC case, $[E_{Cb}]_P$ steeply increases with increasing $d$, because this term is dominated by the additional repulsive interaction between the negatively-charged backbone phosphate groups on the central DNA molecule and the corresponding groups on its periodic replicas. The periodicity-induced perturbation of the Coulomb energy $\Delta E_{Cb}$ (not shown) is thus positive for $d > 0.2$ nm and rapidly increases with increasing $d$ to reach a value of 703 kJ/mol at $d = 1.5$ nm. The Coulomb contributions to the PMF for separating the DNA strands in the presence of counter-ions are displayed in Fig. 8b. In contrast to the previous case, the $[E_{Cb}]_{NP}$ and $[E_{Cb}]_P$ curves have similar shapes. Both increase with increasing $d$ for $d <$ 0.3 nm, corresponding to the disruption of hydrogen bonds between base pairs, and level off beyond this distance. The periodicity-induced perturbation of the Coulomb energy, $\Delta E_{Cb}$ (not shown), is large (approx. 642 kJ/mol) but only weakly sensitive to $d$, increasing quasi-linearly by 1 kJ/mol from $d = 0$ to $d = 1.5$ nm.

The solvation contributions to the PMF in the absence of counter-ions are displayed in Fig. 8c. The contribution $[\Delta G_{self}]_P$ to $[\Delta G'_{solv}]_P$ is a constant evaluating to $-2815$ kJ/mol. Under NPBC, $[\Delta G_{solv}]_{NP}$ is an increasing function of $d$, except between 0.25 and 0.4 nm. This increase can be understood by analogy with the Born model [77]. The dependence of the electrostatic solvation free energy on the square of the solute charge causes a less favorable solvation for two separated DNA strands (charge $-4\ e$) compared to a double-stranded DNA molecule (charge $-8\ e$). The slight decrease between 0.25 and 0.4 nm is a consequence of the definition of the solute–solvent dielectric boundary as a probe-accessible surface. In this range of distance, the nucleotide bases become suddenly accessible to the solvent, causing the decrease in the solvation free energy. Under EWBC, an increase in the distance between the strands corresponds to a decrease in the distance between the negatively-charged phosphate groups on the central DNA molecule and the corresponding groups on its periodic replicas. Consequently, artificial periodicity reverses the dependence of the solvation contribution on $d$, and $[G'_{solv}]_P$ now decreases with increasing $d$ over the whole range of distances. The periodicity-induced perturbation of the solvation free energy, $\Delta\Delta G'_{solv}$ (not shown), is thus negative and rapidly increases in magnitude with increasing $d$ to reach a value of $-743$ kJ/mol at $d = 1.5$ nm. The solvation contributions to the PMF for separating the DNA strands in the presence of counter-ions are displayed in Fig. 8d. The contribution $[\Delta G_{self}]_P$ to $[\Delta G'_{solv}]_P$ is a constant evaluating to $-3209$ kJ/mol. The $[\Delta G_{solv}]_{NP}$ and $[\Delta G'_{solv}]_P$ curves differ significantly only at large separations. The periodicity-induced perturbation of the solvation contribution, $\Delta\Delta G'_{solv}$ (not shown), is positive. For values of $d$ between 0 and 0.7 nm, it is small and moderately sensitive to $d$, varying from 2.9 to 1.9 kJ/mol over this range. Beyond this distance, it raises quickly towards a value of 14.8 kJ/mol at $d = 1.5$ nm.

The curves representing the total electrostatic contributions to the PMF, $\Delta G_{el}$, are displayed in Fig. 9a. The value of $\Delta G_{el}$ at $d = 0$ has been subtracted for easier comparison. In the absence of counter-ions, and in spite of the very different behavior of the Coulomb and solvation contributions under NPBC and EWBC (Fig. 8a,c), the shapes of the $[\Delta G_{el}]_{NP}$ and $[\Delta G_{el}]_P$ curves look surprisingly similar. The double-stranded conformation is electrostatically favored compared to dissociated strands by approximately 28 and 30 kJ/mol under EWBC and NPBC, respectively, as measured between $d = 0$ and $d = 0.6$ nm. A barrier of approximately 154–155 kJ/mol separates these conformations. Here again, this barrier should not be taken too seriously due to the one-parameter pathway considered here. The $[\Delta G_{el}]_P$ curve is shifted down by approximately 51 kJ/mol with respect to the $[\Delta G_{el}]_{NP}$ curve (see the values of these terms at $d = 0$, legend of Fig. 9). Such a negative shift is qualitatively similar to the negative shifts in the electrostatic free energy

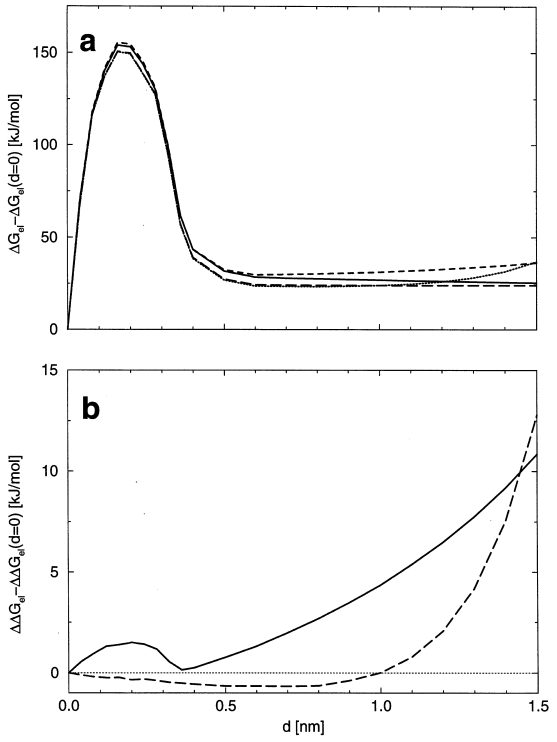


Fig. 9. Periodicity-induced perturbation of the PMF for the separating the strands of the DNA tetranucleotide. The total electrostatic free energy (a), and the periodicity-induced perturbation of this free energy (b), are displayed as a function of the strand-to-strand distance $d$ for the DNA tetranucleotide 3′-TCGA-5′. See legend of Fig. 8. (a) Total electrostatic free energy in the absence of counter ions, $[\Delta G_{el}]_{NP}$ (———) and $[\Delta G_{el}]_P$ (-----), or in the presence of counter-ions, $[\Delta G_{el}]_{NP}$ ( — — —) and $[\Delta G_{el}]_P$ (.....), see Eq. (1); (b) perturbation of the total electrostatic free energy: $\Delta\Delta G_{el}$ from Eq. (1) in the absence (———) or presence (— — —) of counter-ions. For readability, the values of $\Delta G_{el}$ (a) or $\Delta\Delta G_{el}$ (b) at $d = 0$ have been subtracted. These evaluate to $[\Delta G_{el}]_{NP} = -2525$, $[\Delta G_{el}]_P = -2576$, and $\Delta\Delta G_{el} = -51$ kJ/mol in the absence of counter-ions, and $[\Delta G_{el}]_{NP} = -5846$, $[\Delta G_{el}]_P = -6486$, and $\Delta\Delta G_{el} = -640$ kJ/mol in the presence of counter-ions.

observed for spherical ions [58]. Although the inclusion of counter-ions results in very different Coulomb and solvation contributions (Fig. 8b,d), the curves representing the total electrostatic PMF are strikingly similar to those obtained in the absence of counter-ions. Note, however, that the $[\Delta G_{el}]_P$ curve is now shifted down by approximately 640 kJ/mol with respect to the $[\Delta G_{el}]_{NP}$ curve.

The curves representing the periodicity-induced perturbation of the PMF, $\Delta\Delta G_{el}$, are displayed in Fig. 9b. The value of $\Delta\Delta G_{el}$ at $d = 0$ has been subtracted for easier comparison. In the absence of counter-ions, artificial periodicity raises the barrier by approximately 1 kJ/mol. Above $d = 0.35$ nm, the Coulomb effect dominates over the solvation effect and $\Delta\Delta G_{el} - \Delta\Delta G_{el}(d = 0)$ increases quickly with distance to reach a value of 10.9 kJ/mol at $d = 1.5$ nm. The inclusion of artificial periodicity under EWBC thus provides a strong additional stabilization of the double-stranded configuration with respect to the dissociated strands. In contrast, in the presence of explicit counter-ions, the perturbation of the electrostatic PMF is dominated by the perturbation of the solvation contribution. $\Delta\Delta G_{el} - \Delta\Delta G_{el}(d = 0)$ slowly decreases for $d < 0.7$ nm, down to a value of $-0.7$ kJ/mol. Beyond this distance the curve increases steeply with increasing $d$ to reach a value of 12.8 kJ/mol at $d = 1.5$ nm. Thus, in this case the periodicity-induced perturbation results in a limited destabilization of the double-stranded configuration with respect to configurations with a small separation of the strands ($d < 0.7$ nm), but a strong stabilization of the double-stranded configuration with respect to the dissociated strands at large separations.

### 4.4. Sac7d

Correlations between (free) energy contributions corresponding to 180 solute configurations sampled during the explicit-solvent MD simulation of the protein Sac7d at 550 K under EWBC [67] are presented in Fig. 10. The contribution $[\Delta G_{self}]_P$ is a constant and evaluates to $-1998$ kJ/mol. Parameters obtained from a least-squares fit corresponding to these and other correlations are reported in Table 1. The correlation between the Coulomb energies $[E'_{Cb}]_P$ and $[E_{Cb}]_{NP}$, is displayed in Fig. 10a. Since the intramolecular Coulomb energy generally increases during the unfolding of a protein, the direction of the unfolded state is towards the right of the graph. The linear correlation is good ($r = 0.992$) and the calculated slope is 0.9989. This slope corresponds to a periodicity-induced destabilization of the folded

structure ($\min\{[E_{Cb}]_{NP}\}$) with respect to the most unfolded structure observed in the simulation ($\max\{[E_{Cb}]_{NP}\}$) by $\delta_x - \delta_y = 1.7$ kJ/mol. The correlation between the solvation free energies $[\Delta G_{solv}]_P$ and $[\Delta G_{solv}]_{NP}$, is presented in Fig. 10b. Since the solvation free energy will generally become more negative upon unfolding, the direction of the unfolded state is now towards the left of the graph. The linear correlation is also good ($r = 0.991$) and the calculated slope is 0.9963. This slope corresponds to a periodicity-induced stabilization of the folded structure ($\max\{[\Delta G_{solv}]_{NP}\}$) with respect to the most unfolded structure observed in the simulation ($\min\{[\Delta G_{solv}]_{NP}\}$) by $\delta_y - \delta_x = 5.7$ kJ/mol. Since the folded state is stabilized by 5.7 kJ/mol in the solvation contribution, and destabilized by only 1.7 kJ/mol in the Coulomb contribution, the overall periodicity-induced stabilization is 4.0 kJ/mol. This estimate relies on the assumption that the degree of unfolding can be monitored through $[E_{Cb}]_{NP}$ or through $[\Delta G_{solv}]_{NP}$, and that for any configuration, a high value of the former quantity implies a low value of the latter. The validity of this assumption is supported by the good correlation ($r = -0.989$) between $[\Delta G_{solv}]_{NP}$ and $[E_{Cb}]_{NP}$, with a slope close to minus one ($-0.9122$).

Other estimates for the periodicity-induced perturbation can be obtained from the correlations of $[\Delta G_{el}]_{NP}$ or $[\Delta G_{el}]_P$, with $[E_{Cb}]_{NP}$ or $[\Delta G_{solv}]_{NP}$. The slopes corresponding to the correlations of $[\Delta G_{el}]_{NP}$ and $[\Delta G_{el}]_P$ with $[E_{Cb}]_{NP}$ differ by 0.0017, which corresponds to an artificial stabilization of the folded state by 2.9 kJ/mol (i.e. the difference between $\delta_y$ for these two correlations). For the correlations of $[\Delta G_{el}]_{NP}$ and $[\Delta G_{el}]$ with $[\Delta G_{solv}]_{NP}$, the slopes differ by 0.0020, which corresponds to an artificial stabilization of the folded state by 3.0 kJ/mol. These estimates agree well with the above number of 4.0 kJ/mol.

A perturbation of 3–4 kJ/mol (0.7–0.9 $k_B T$ at 550 K) may appear small at first sight. However, since conformations were sampled by MD under EWBC, the sampling of unfolded conformations with a periodicity-induced destabilization larger than approximately $k_B T$ is unlikely. Consequently, the observed perturbation is about the maximal perturbation that one can expect to observe in this case, and the artifactual stabilization of the folded state is certainly significant. Of course, a larger effect might be observed if the configurations are generated by MD simulation using cutoff truncation instead of the $P_3M$ method. Such a study is in progress.

Finally, we note the good correlation ($r = 0.920$)

Table 1
Correlations between (free) energy contributions calculated for 180 Sac7d configurations

| $Q_1$ | $Q_2$ | $r$ | $a$ | $b$ (kJ/mol) | $\delta_x$ (kJ/mol) | $\delta_y$ (kJ/mol) |
|---|---|---|---|---|---|---|
| $[E_{Cb}]_{NP}$ | $[E'_{Cb}]_P$ | 0.992 | 0.9989 | −1174.5 | 1652.2 | 1650.5 |
| $[\Delta G_{solv}]_{NP}$ | $[\Delta G_{solv}]_P$ | 0.991 | 0.9963 | 1123.8 | 1529.2 | 1523.5 |
| $[E_{Cb}]_{NP}$ | $[\Delta G_{solv}]_{NP}$ | −0.989 | −0.9122 | −10793.9 | 1652.2 | −1507.2 |
| $[E'_{Cb}]_P$ | $[\Delta G_{solv}]_P$ | −0.990 | −0.9108 | −10704.8 | 1688.8 | −1538.2 |
| $[E_{Cb}]_{NP}$ | $[\Delta G_{el}]_{NP}$ | 0.548 | 0.0878 | −10793.9 | 1652.2 | 145.0 |
| $[E_{Cb}]_{NP}$ | $[\Delta G_{el}]_P$ | 0.555 | 0.0895 | −10807.5 | 1652.2 | 147.9 |
| $[G_{solv}]_{NP}$ | $[\Delta G_{el}]_{NP}$ | −0.420 | −0.0730 | −11676.6 | 1529.2 | −111.7 |
| $[\Delta G_{solv}]_{NP}$ | $[\Delta G_{el}]_P$ | −0.429 | −0.0750 | −11711.3 | 1529.2 | −114.7 |
| $[\Delta G_{solv}]_P$ | $\frac{1}{2}E_{ps}^{sim}$ | 0.920 | 1.0331 | 363.8 | 1563.5 | 1615.2 |

Correlations between the two quantities $Q_1$ and $Q_2$ are given in the form of parameters issued from a least-square fit of $Q_2 = f(Q_1)$ to a straight line: correlation coefficient ($r$), slope ($a$), intercept $Q_2$ at $Q_1 = 0$ (b). $\delta_x$ and $\delta_y$ are defined as $\delta_x \equiv \max\{Q_1\} - \min\{Q_1\}$ and $\delta_y \equiv (a \cdot \max\{Q_1\} + b) - (a \cdot \min\{Q_1\} + b)$, where min $\{Q_1\}$ and max $\{Q_1\}$ denote the minimal and maximal values of $Q_1$. The different quantities $Q_1$ and $Q_2$ are defined in Eq. (1). Primed quantities include the self-term $[\Delta G_{self}]_P = -1998$ kJ/mol. $E_{ps}^{sim}$ is the protein–solvent energy monitored during the explicit-solvent MD simulation. This quantity was calculated by subtracting from the Ewald energy [Eq. (9)] corresponding to the protein and solvent charges, the Ewald energies corresponding to the protein charges alone and to the solvent charges alone [67].

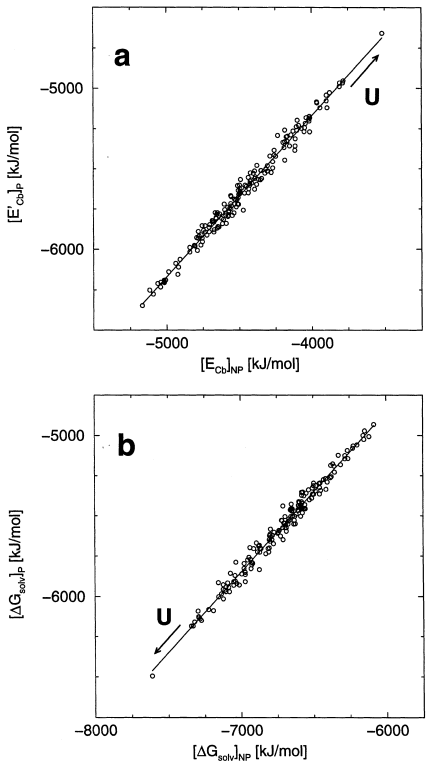


Fig. 10. Periodicity-induced perturbation of the electrostatic (free) energy contributions for Sac7d. Correlations between (free) energy contributions under NPBC and EWBC are displayed for 180 conformations of the protein. Correlations of (a) $[E'_{Cb}]_P \equiv [E_{Cb}]_P + [\Delta G_{self}]_P$, from Eqs. (9) and (10), with $[E_{Cb}]_{NP}$ from Eq. (8); (b) $[\Delta G_{solv}]_P$ from Eq. (6) and $[\Delta G_{solv}]_{NP}$ from Eq. (3); regression parameters for these and other correlations are reported in Table 1. The symbol $U$ indicates the direction of the unfolded state.

between $[\Delta G_{solv}]_P$, as obtained from the continuum calculation, and the protein–solvent interaction energy divided by two, $1/2E_{ps}^{sim}$, as monitored during the explicit-solvent simulation. The calculated slope is very close to unity (1.0331). Such a correlation with unit slope is expected if the polarization of the solvent is linear in the applied electrostatic field (linear-response), and so long as instantaneous solvent configurations can be compared with the (time-averaged) continuum representation. The excellent correlation indicates that both conditions are met in the present case. This, of course, is likely to be a consequence of the net charge of the protein ($-6\ e$), which is small enough to avoid dielectric saturation of the solvent, yet large enough to impose a strong electric field around the protein.

## 5. Conclusion

In the present study we investigated, using continuum electrostatics, the nature and magnitude of artifacts linked with the use of the Ewald and related ($P_3M$, PME, FMM) methods in explicit-solvent simulations. The results indicate that artificial periodicity imposed by the use of Ewald boundary conditions (EWBC) instead of non-periodic boundary conditions (NPBC) may significantly perturb the electrostatic PMFs for conformational equilibria of solvated biomolecules.

For polyalanine oligopeptides with neutral termini in water, artificial periodicity results in a limited ($< 0.3$ kJ/mol) additional stabilization of the $\alpha$-helical conformation with respect to more extended ones. Due to the small magnitude of this effect, the use of EWBC in an explicit-solvent simulation is unlikely to affect significantly the conformational equilibria of such oligopeptides. In contrast, when the termini of the oligopeptides are charged, the periodicity-induced perturbation results in a large increase in the electrostatic free energy of extended conformations. Under NPBC, the electrostatic free energies of the extended conformations (at the minimum of the PMF) are always lower than those of the $\alpha$-helical conformations. Under EWBC, and for a cubic unit cell of edge $L = 4$ nm, the corresponding (negative) free energy differences are increased by 1.1, 1.1, and 3.6 kJ/mol, for the hexa-, octa-, and decapeptide, respectively. The use of EWBC in an explicit-solvent simulation is thus likely to significantly bias the conformational equilibria of oligopeptides with charged termini. Such conformational artifacts are strongly dependent on the unit cell size, in this specific case proportional to $L^{-5}$, and we estimate that in the case of the octapeptide, a box of edge of at least 4.3 nm is required to keep the effect of the perturbation below $k_BT$. We are also currently investigating whether such a box-size dependence can be

observed in explicit-solvent MD simulations.

For a DNA tetranucleotide in the absence of counter-ions, artificial periodicity also results in a strong (up to 10.9 kJ/mol for $L = 4$ nm) additional stabilization of the double-stranded configuration with respect to the separated strands. In the presence of explicit counter-ions, the periodicity-induced perturbation results in a limited ($< 0.7$ kJ/mol for $L = 4$ nm) destabilization of the double-stranded configuration with respect to configurations with a small separation between the strands ($d < 0.7$ nm), but a strong (up to 12.8 kJ/mol for $L = 4$ nm) stabilization of the double-stranded configuration with respect to the dissociated strands at large separations.

Finally, the analysis of 180 conformations sampled during a 0.9-ns MD simulation of the protein Sac7d at 550 K using the $P_3M$ method reveals a periodicity-induced stabilization of the folded state with respect to the most unfolded state observed during the simulation by 3–4 kJ/mol (0.7–0.9 $k_BT$). Since the sampling of unfolded conformations with a periodicity-induced destabilization larger than about $k_BT$ is unlikely in an explicit-solvent simulation under EWBC, this artifactual destabilization of unfolded conformations is certainly significant. Therefore the use of EWBC is probably in large part responsible for the unexpected stability of the protein during the simulation.

From this and a previous study [58], we can discuss the factors controlling the magnitude of artifacts linked with the use of EWBC. The periodicity-induced perturbation of an electrostatic PMF is often reduced by a significant cancellation between much larger perturbations in the Coulomb and solvation contributions. This cancellation will be most effective in the presence of a solvent of high dielectric permittivity (e.g. water), and when the ratio of the size of the low-dielectric solute cavity to the size of the unit cell is small (e.g. small spherical ions [58]). If a solvent of low permittivity is considered, the perturbation in the Coulomb term will dominate, and large periodicity-induced artifacts can be expected. Indeed, when the permittivity of the solvent is unity (vacuum), solvation effects will completely vanish. Even in a solvent of high permittivity, artifacts may arise when the size of the low-dielectric cavity is not negligible compared to the size of the unit cell. This is the case for all biomolecular systems considered in the present study. Depending on the system, the imbalance between the perturbations in the Coulomb and solvation terms may result in a dominance of the Coulomb term (e.g. oligopeptides with neutral termini and the tetranucleotide without counter-ions), or of the solvation term (e.g. oligopeptides with charged termini, the tetranucleotide with counter-ions, and Sac7d). However, irrespective of which term dominates, artificial periodicity always stabilizes the most compact form of the biomolecule. If this turns out to be a general feature of periodicity-induced perturbation, artificial periodicity may be one cause for the high stability of the native conformations of biomolecules observed in explicit-solvent simulations under EWBC [31–33,45,46]. Finally, the magnitude of the artifact is correlated with the number, magnitude and locations of the charges in the system. This correlation is, however, not straightforward. As evidenced by the oligopeptides with charged termini, neither the neutrality of the solute nor the absence of charges at distances exceeding half the unit cell size do guarantee the absence of artifacts. On the other hand, the presence of a non-neutral solute seems to always be associated with the presence of artifacts.

Although Ewald and related methods are formally exact for periodic systems, they are only approximate for simulating solutions, since solutions are inherently non-periodic. The present study shows that artificial periodicity may induce strong perturbations in the PMFs for conformational equilibria of biomolecules in solution. Our method based on continuum electrostatics allows to identify and estimate the magnitude of these artifacts. It is our hope that this knowledge will trigger further improvements of Ewald and related methods, with the aim of relaxing the requirement of periodicity [78].

## Acknowledgements

PHH would like to thank Valérie Dillet, Wolf-

gang Weber and Adrian Elcock for their critical reading of the manuscript, Paul de Bakker for providing the Sac7d trajectory, and acknowledges support from the Swiss National Fund and the Human Frontier Science Program. Additional support was provided by NIH and NSF. This work was also partially supported by the NSF Supercomputer Centers NRAC program.

## References

[1] S.C. Harvey, Proteins: Struct. Funct. Genet. 5 (1989) 78.
[2] M.E. Davis, J.A. McCammon, Chem. Rev. 90 (1990) 509.
[3] H.J.C. Berendsen, in: W.F. van Gunsteren, P.K. Weiner, A.J. Wilkinson (Eds.), Electrostatic Interactions (Computer Simulation of Biomolecular Systems, Theoretical and Experimental Applications, vol. II, ESCOM, Leiden, 1993, p. 161.
[4] P.E. Smith, W.F. van Gunsteren, in: W.F. van Gunsteren, P.K. Weiner, A.J. Wilkinson (Eds.), Methods for the Evaluation of Long Range Electrostatic Forces in Computer Simulations of Molecular Systems (Computer simulation of biomolecular systems, theoretical and experimental applications, vol. II, ESCOM, Leiden, 1993, p. 182.
[5] R.M. Levy, E. Gallicchio, Annu. Rev. Phys. Chem. 49 (1998) 531.
[6] M.P. Allen, D.J. Tildesley, Computer Simulation of Liquids, Oxford University Press, New York, 1987.
[7] S.W. de Leeuw, J.W. Perram, E.R. Smith, Proc. R. Soc. London, Ser A 373 (1980) 27.
[8] A.Y. Toukmaji, J.A. Board, Jr., Comput. Phys. Commun. 95 (1996) 73.
[9] R.W. Hockney, J.W. Eastwood, Computer Simulation using Particles, Institute of Physics Publishing, Bristol, 1988.
[10] B.A. Luty, M.E. Davis, I.G. Tironi, W.F. van Gunsteren, Mol. Sim. 14 (1994) 11.
[11] B.A. Luty, I.G. Tironi, W.F. van Gunsteren, J. Chem. Phys. 103 (1995) 3014.
[12] T. Darden, D. York, L. Pedersen, J. Chem. Phys. 98 (1993) 10089.
[13] U. Essmann, L. Perera, M.L. Berkowitz, T. Darden, H. Lee, L.G. Pedersen, J. Chem. Phys. 103 (1995) 8577.
[14] H.G. Petersen, J. Chem. Phys. 103 (1995) 3668.
[15] C.A. White, M. Head-Gordon, J. Chem. Phys. 101 (1994) 6593.
[16] F. Figueirido, R.M. Levy, R. Zhou, B.J. Berne, J. Phys. Chem. 106 (1997) 9835.
[17] M. Challacombe, C. White, M. Head-Gordon, J. Chem. Phys. 107 (1997) 10131.
[18] M. Neumann, Mol. Phys. 50 (1983) 841.
[19] M. Neumann, O. Steinhauser, G.S. Pawley, Mol. Phys. 52 (1984) 97.
[20] C.L. Brooks III, J. Chem. Phys. 86 (1987) 5156.
[21] J.D. Madura, B.M. Pettitt, Chem. Phys. Lett. 150 (1988) 105.
[22] T.P. Straatsma, H.J.C. Berendsen, J. Chem. Phys. 89 (1989) 5876.
[23] R.H. Wood, J. Chem. Phys. 103 (1995) 6177.
[24] B.M. Pettitt, P.J. Rossky, J. Chem. Phys. 84 (1986) 5836.
[25] L.X. Dang, B.M. Pettitt, J. Phys. Chem. 94 (1990) 4303.
[26] E. Guàrdia, R. Rey, J.A. Padró, J. Chem. Phys. 95 (1991) 2823.
[27] L.X. Dang, B.M. Pettitt, P.J. Rossky, J. Chem. Phys. 96 (1992) 4046.
[28] J.S. Bader, D. Chandler, J. Phys. Chem. 96 (1992) 6423.
[29] G. Hummer, D.M. Soumpasis, M. Neumann, Mol. Phys. 81 (1993) 1155.
[30] G.S. Del Buono, F.E. Figueirido, R.M. Levy, Chem. Phys. Lett. 263 (1996) 521.
[31] P.E. Smith, B.M. Pettitt, J. Chem. Phys. 95 (1991) 8430.
[32] H. Schreiber, O. Steinhauser, Biochemistry 31 (1992) 5856.
[33] H. Schreiber, O. Steinhauser, Chem. Phys. 168 (1992) 75.
[34] H. Schreiber, O. Steinhauser, J. Mol. Biol. 228 (1992) 909.
[35] R.J. Loncharich, B.R. Brooks, Proteins: Struct. Funct. Genet. 6 (1989) 32.
[36] P.J. Steinbach, B.R. Brooks, J. Comput. Chem. 15 (1994) 667.
[37] J.A. Barker, R.O. Watts, Mol. Phys. 26 (1973) 789.
[38] H. Alper, R.M. Levy, J. Chem. Phys. 91 (1989) 1242.
[39] G. Hummer, D.M. Soumpasis, J. Phys.: Condens. Matter 6 (1994) A141.
[40] I.G. Tironi, R. Sperb, P.E. Smith, W.F. van Gunsteren, J. Chem. Phys. 102 (1995) 5451.
[41] P.H. Hünenberger, W.F. van Gunsteren, J. Chem. Phys. 108 (1998) 6117.
[42] G.S. Del Buono, T.S. Cohen, P.J. Rossky, J. Mol. Liq. 60 (1994) 221.
[43] K.F. Lau, H.E. Alper, T.S. Thatcher, T.E. Stouch, J. Phys. Chem. 98 (1994) 8785.
[44] L. Perera, U. Essmann, M.L. Berkowitz, J. Chem. Phys. 102 (1994) 450.
[45] D.M. York, T.A. Darden, L.G. Pedersen, J. Chem. Phys. 99 (1993) 8345.
[46] T. Fox, P.A. Kollman, Proteins: Struct. Funct. Genet. 25 (1996) 315.
[47] V. Mohan, P.E. Smith, B.M. Pettitt, J. Phys. Chem. 97 (1993) 12984.
[48] T.E. Cheatham III, P.A. Kollman, J. Mol. Biol. 259 (1996) 434.
[49] T.E. Cheatham III, P.A. Kollman, Structure 5 (1997) 1297.
[50] T.E. Cheatham III, M.F. Crowley, T. Fox, T. Kollman, P.A. Kollman, Proc. Natl. Acad. Sci. USA 94 (1997) 9626.
[51] M.A. Young, G. Ravishanker, D.L. Beveridge, Biophys. J. 73 (1997) 2313.

[52] P. Auffinger, E. Westhof, J. Mol. Biol. 269 (1996) 326.
[53] P. Auffinger, E. Westhof, Curr. Opin. Struct. Biol. 8 (1998) 227.
[54] P.E. Smith, B.M. Pettitt, J. Chem. Phys. 105 (1996) 4289.
[55] G. Hummer, L.R. Pratt, A.E. Garcia, J. Phys. Chem. 100 (1996) 1206.
[56] F. Figueirido, G.S. Del Buono, R.M. Levy, J. Phys. Chem. B 101 (1997) 5622.
[57] G. Hummer, L.R. Pratt, A.E. Garcia, J. Chem. Phys. 107 (1997) 9275.
[58] P.H. Hünenberger, J.A. McCammon, J. Chem. Phys. 101 (1999) 1856.
[59] B.R.A. Nijboer, T.W. Ruijgrok, J. Stat. Phys. 53 (1988) 361.
[60] B. Cichocki, B.U. Felderhof, K. Hinsen, Phys. Rev. A 39 (1989) 5350.
[61] G. Hummer, D.M. Soumpasis, J. Chem. Phys. 98 (1993) 581.
[62] F. Figueirido, G.S. Del Buono, R.M. Levy, J. Chem. Phys. 103 (1995) 6133.
[63] O. Norberto de Souza, R.L. Ornstein, Biophys. J. 72 (1997) 2395.
[64] T.R. Reddy, T. Suryanarayana, Biochem. Biophys. Acta 949 (1988) 87.
[65] J.G. McAfee, S.P. Edmondson, P.K. Datta, J.W. Shriver, R. Gupta, Biochemistry 34 (1995) 10063.
[66] S.P. Edmondson, L. Qiu, J.W. Shriver, Biochemistry 34 (1995) 13289.
[67] P.I.W. de Bakker, P.H. Hünenberger, J.A. McCammon, J. Mol. Biol. 285 (1999) 1811.
[68] J.D. Madura, M.E. Davis, M.K. Gilson, R.C. Wade, B.A. Luty, J.A. McCammon, in: K.B. Lipkowitz, D.B. Boyd (Eds.), Biological Applications of Electrostatic Calculations and Brownian Dynamics Simulations (Reviews in computational chemistry, vol. 4), VCH, New York, 1994, p. 229.
[69] MOLECULAR SIMULATION INC., Quanta version 4.0 parameter handbook. 200 Fifth Avenue, Waltham, MA 02154 (1992).
[70] D.S. Goodsell, K. Grzeskowiak, R.E. Dickerson, Biochemistry 34 (1995) 1022.
[71] W.F. van Gunsteren, S.R. Billeter, A.A. Eising et al. Biomolecular Simulation: The GROMOS96 Manual and User Guide, Verlag der Fachvereine, Zürich, 1996.
[72] V. Daggett, M. Levitt, J. Mol. Biol. 232 (1993) 600.
[73] J. Tirado-Rives, W.L. Jorgensen, Biochemistry 32 (1993) 4175.
[74] P.H. Hünenberger, A.E. Mark, W.F. van Gunsteren, Proteins: Struct. Funct. Genet. 21 (1995) 196.
[75] A. Caflisch, M. Karplus, J. Mol. Biol. 252 (1995) 672.
[76] L. Onsager, J. Am. Chem. Soc. 58 (1936) 1486.
[77] M. Born, Z. Phys. 1 (1920) 45.
[78] B.A. Luty, W.F. van Gunsteren, J. Phys. Chem. 100 (1996) 2581.